AIP Journal of Applied Physics

The influence of void space on antireflection coatings of silica nanoparticle self-assembled films

S. E. Yancey, W. Zhong, J. R. Heflin, and A. L. Ritter

Citation: Journal of Applied Physics **99**, 034313 (2006); doi: 10.1063/1.2171784
View online: http://dx.doi.org/10.1063/1.2171784
View Table of Contents: http://scitation.aip.org/content/aip/journal/jap/99/3?ver=pdfcov
Published by the AIP Publishing

The influence of void space on antireflection coatings of silica nanoparticle self-assembled films

S. E. Yancey, W. Zhong, J. R. Heflin, and A. L. Ritter[a)]
Department of Physics, Virginia Tech, Blacksburg, Virginia 24061

(Received 27 July 2005; accepted 11 January 2006; published online 15 February 2006)

This study investigates the deposition by ionic self-assembly of alternating silica nanoparticle and poly(allyamine hydrochloride) layers with the goal to create a single-material antireflection coating. The condition that the optical thickness of the film be equal to $\lambda/4$ can be satisfied by depositing the requisite number of bilayers to obtain minimum reflectivity at the chosen wavelength. The second condition for antireflection, that the index of refraction of the film be equal to $n_c=\sqrt{n_1 n_2}$, where n_1 and n_2 are the refractive indices of the media on each side of the film, requires that $n_c=1.22$ for a film with air on one surface and glass (assuming $n=1.50$) on the other. Such a low index of refraction can be created in films consisting of nanoparticles if the proper volume fraction of void space exists in the film. In the wavelength range $\lambda=350-700$ nm, minimum reflectivities of $\geqslant 2.0\%$, $\leqslant 0.2\%$, and $\leqslant 0.2\%$ were obtained with films created on both sides of a glass slide using 15, 45, and 85 nm average diameter silica nanoparticles, respectively. The maximum transmittances for the corresponding films were 97%, $\geqslant 98\%$, and $\geqslant 97\%$. The minimum reflectance of films prepared with 15 nm average diameter silica nanoparticles was limited by insufficient void volume in the films. The maximum transmittances of films prepared with 45 and 85 nm average diameter silica nanoparticles were limited by diffuse scattering arising from the inhomogeneous morphology of the films. The extinction of normal incident light ($=1-R-T$, where R and T are the reflectance and transmittance, respectively) provides a measure of diffuse scattering for light with wavelength longer than the absorption edge of the film. It was found that the extinction is proportional to $1/\lambda^4$ for $\lambda>450$ nm suggesting that the mechanism for extinction at long wavelengths is Rayleigh scattering. The Rayleigh slope (diffuse scattering intensity versus $1/\lambda^4$) increased with increasing diameter silica nanoparticles. For a given average diameter silica nanoparticle, the Rayleigh slope increased with increasing film thickness for films less than approximately 150 nm thick, but did not depend on film thickness, within experimental scatter, for films that were thicker than 150 nm. The results suggest that the source of Rayleigh scattering was not in the bulk of the film (such as, fluctuations in the index of refraction), but rather was primarily associated with surface roughness. © *2006 American Institute of Physics*. [DOI: 10.1063/1.2171784]

I. INTRODUCTION

We report studies of the reflectivity and transmission in the visible range ($\lambda=350-700$ nm) of thin films created by ionic self-assembly of alternating layers of silica nanoparticles and the polycation poly(allyamine hydrochloride) (PAH) as a function of nanoparticle size and deposition conditions. The purpose of this study is to provide deeper understanding of the relationship between the packing of the silica nanoparticles in the layers and the optical characteristics of the films. In order to minimize the reflectivity of incident light at a given wavelength λ (antireflection coating), the deposited film must satisfy the two conditions: (1) the optical thickness (thickness times the index of refraction) of the film is equal to $\lambda/4$ and (2) the index of refraction of the film is equal to $n_c=\sqrt{n_1 n_2}$, where n_1 and n_2 are the refractive indices of the media on each side of the film. The optical thickness of our films can be controlled by the number of alternating layers that are deposited. The second condition is generally more difficult to satisfy. An antireflection (AR) coating for glass (assuming $n=1.50$) surrounded by air should ideally have a refractive index of 1.22. Such a low refractive index is not possible to achieve with homogeneous materials. A commonly used AR coating, MgF_2 ($n=1.38$), reduces the reflectivity from 4% for a single glass/air interface to ~1.5%. It is clearly desirable to have an inexpensive method for fabricating lower refractive index films that would reduce the reflectivity further. One possible approach for achieving the desired index of refraction is to deposit an inhomogeneous film consisting of a controlled fraction of void space ($n=1.0$) in a low refractive index material. However, the variation in the size and spacing of these voids results in diffuse scattering that degrades the quality of the AR coating. This conflict, between using inhomogeneous films to achieve the desired index of refraction and the concomitant diffuse scattering, is examined in this paper.

The ionic self-assembly of particles from a colloidal suspension first was demonstrated by Iler[1] who deposited layers of oppositely charged particles and characterized the thicknesses of the resulting films by the color of the reflected light. The scope of the technique was expanded significantly by Lvov and Decher[2] and Decher[3] who demonstrated that

[a)]Electronic mail: aritter@vt.edu

polyelectrolytes could be efficiently employed in layer-by-layer assembly. The self-assembly of nanoparticles has been reviewed by Kotov,[4] and the broader context of electrostatic multilayer thin film assembly is reviewed by Hammond.[5] The layer-by-layer ionic self-assembly of silica nanoparticles has been studied extensively.[6–12] Three of these studies[7,10,11] found that the indices of refraction of alternating layers of silica nanoparticles and polycations were in the range $n=1.25-1.36$ and, therefore, these films potentially could be used for AR coatings. Hattori[10] demonstrated that a single bilayer of silica nanoparticles/polycation could be an AR coating, but tuning the minimum reflectivity of this film required different size nanoparticles.

The index of refraction of films assembled from silica nanoparticles and a polycation is significantly less than the indices of refraction of both materials because empty space ($n=1.0$) exists between the polycation-covered silica spheres. If the contacting spheres are monodispersed and form a random closed-packed (RCP) structure, then the volume fraction of silica is 64% leaving 36% void. The theoretical index of refraction in the effective-medium approximation of such a RCP mixture of silica and void space is 1.3, assuming that the extinction coefficient is negligible. We find in this study that the index of refraction of silica nanoparticles/polycation films made with 45 nm average diameter silica nanoparticles can be less than an ideal RCP film because in the first few bilayers, the nanoparticles aggregate in small islands. The void space between the islands is roughly the same size as the aggregates and significantly larger than the void space between RCP spheres. As a consequence, the void space fraction in films with less than three or four bilayers is greater than 0.36 and, concomitantly, the index of refraction is less than 1.3. As more layers are deposited, the void space between aggregates apparently fills in and the index of refraction increases towards 1.4.

Lvov *et al.*[9] investigated the deposition of alternating silica nanoparticles and poly(diallyldimethylammonium chloride) (PDDA) polycation layers and found that the deposition of each layer is highly reproducible and that the ratio of the change in average bilayer thickness to the average diameter of the silica nanoparticle depended on the silica suspension concentration and on the time that the substrate was left in the suspension. The question then arises whether the observed surface coverage at constant dip time is an equilibrium adsorption isotherm. In another quartz-crystal microbalance (QCM) study, Lvov *et al.*[11] monitored the mass deposition of PDDA and silica nanoparticles on a silver electrode as a function of time for a silica suspension concentration of 10 mg/ml. For a total deposition period of ~180 s, 90% of the final mass of silica was deposited on the electrode in the first 10 s. The adsorption continued at a very low rate up to the end of the deposition period. This nonlinear time dependence of adsorption of particles from solution on to a substrate has been studied extensively.[13] A general finding of these studies is that when the Debye screening length for the electrostatic interaction between nanoparticles in the suspension is larger than the nanoparticle diameter (low concentration of counterions in the suspension), then two distinctive regimes are predicted for adsorption of the nanoparticles on a substrate: (1) a fast Langmuir-type adsorption for short times and (2) a very slow approach to the maximum surface concentration for long times. Several model studies of this adsorption process highlight the role of the repulsive electrostatic interaction among adsorbing particles to reduce both the particle adsorption rate and the long-time plateau that defines the maximum surface coverage of the substrate. The nanoparticles that initially adsorb on the surface "block" the subsequent adsorption of nanoparticles from the suspension.

The blocking of nanoparticle adsorption from the suspension by nanoparticles already adsorbed on the surface is a possible mechanism for creating sufficient void spaces in layer-by-layer-assembled films to obtain the necessary low index of refraction. The purpose of this study is to identify the source of diffuse scattering from the inhomogeneous films. We find that the primary source is the surface roughness of the films rather than inhomogeneities in the bulk index of refraction. The challenge, then, is to create the necessary void structure in the bulk film to obtain the required index of refraction for minimum reflection and, at the same time, minimize the surface roughness of the film so that diffuse scattering is not excessive. Even with the diffuse scattering, we obtain peak transmittances higher than those available with single-layer MgF_2 coatings.

Details of the sample preparation and optical measurements are described in Sec. II. The results of the measurements are discussed in Secs. III A–III C. Sections IV A–IV C presents the discussion of our measurements. The results are summarized in Sec. V

II. EXPERIMENTAL DETAILS

The silica nanoparticles used in this study were in colloidal suspensions made by SNOWTEX Nissan Chemical. The typical particle size and range of *p*H stability for the different colloidal suspensions are given in Table I. The suspensions were diluted with de-ionized water (18 MΩ cm resistivity) to obtain the listed concentration of nanoparticles and the *p*H was adjusted to *p*H=7 or 9 with HCl or NH_4OH. The polycation used for these films is PAH from Sigma Aldrich with a typical molecular weight of 15 000. The PAH solutions were adjusted to 10 mM concentration with de-ionized water. The *p*H of the PAH suspensions was adjusted to either *p*H=7 or *p*H=9 with NH_4OH. We will refer to different films as silica(nominal particle sizes=15, 45, or 85 nm; *p*H=7 or 9)/PAH(*p*H=7 or 9).

The glass microscope slide substrates were cleaned by the RCA procedure[14] and then dried with flowing nitrogen gas. Films were deposited on both sides of the microscope slide by alternately dipping it into the PAH and silica nanoparticle solutions. Slides were immersed in each solution for 3 min and rinsed five times with de-ionized (DI) water between each immersion. As can be seen in Table I, the *p*H levels of the silica suspensions and of the PAH solutions were typically below the lower limit of the silica stability range suggested by the manufacturer. When we attempted to fabricate samples at higher *p*H, the quality of the films was degraded.

TABLE I. Characteristics of SNOWTEX nanoparticles suspensions from Nissan are listed in columns two and three. The concentration and *p*H of the silica suspensions used to prepare films are listed in the fourth and fifth columns. The *p*H of the PAH polycation solution is listed in the sixth column.

SNOWTEX type	Typical particle size (nm)	Silica min/max stable *p*H	Concentration (mg/ml)	Silica *p*H	PAH *p*H
ST-C	15	8.5/9.0	110	7	7
ST-20L	45	9.5/11	45	9	9
ST-20L	45	9.5/11	45	9	7
ST-ZL	85	9.0/10	100	9	9

The reflectivities of the films were measured from $\lambda = 250$ to $\lambda = 850$ nm with a Filmetrics F-20 thin-film measurement system. The incident light from a bundle of six optical fibers was normal to the film and the reflected light was detected by a single optical fiber in the center of the source bundle. The transmittances were measured with a Perkin-Elmer Lambda 25 spectrophotometer.

III. RESULTS

A. Reflectance and transmittance from films prepared with 15, 45, and 85 nm nanoparticles

Starting with films prepared from the smallest size silica nanoparticles, the transmittances of four films (5,10,15, and 20 bilayers) of silica (15 nm; *p*H=7)/PAH(*p*H=7) as a function of wave number (=$1/\lambda$) are shown in Fig. 1. The interference fringes are visible at wave numbers that are less than the absorption edge of the glass substrate (approximately 3.0 μm^{-1}). The interference fringes are more clearly evident in the reflectance of the same samples shown in Fig. 2. The positions of minimum and maximum reflectivities as a function of wavelength and the number of bilayers display expected behavior. When the indices of atmosphere (n_0), film (n_f), and substrate (n_s) are ordered in magnitude $n_0 < n_f < n_s$, then the wave numbers for minimum and maximum reflectivities are given by

$$1/\lambda_{\min} = p/4\mathrm{OT}, \quad p = 1,3, \ldots, \tag{1}$$

$$1/\lambda_{\max} = q/2\mathrm{OT}, \quad q = 1,2, \ldots, \tag{2}$$

where OT is the optical thickness of the film. If the optical thickness is proportional to the number of bilayers, then the first minimum of the ten-bilayer film and the first maximum of the 20-bilayer film should occur at the same wave number. The congruence of these two conditions occurs at approximately 2.3 μm^{-1} in our data. The minimum reflectivity (from both faces) at this wave number for the ten-bilayer film is 2.2%.

For the medium-sized silica nanoparticles, the transmittances as a function of wave number of silica(45 nm; *p*H =9)/PAH(*p*H=7) films having 3, 5, 8, 10, and 15 bilayers are shown in Fig. 3. The reflectance spectra of the same samples are shown in Fig. 4. The positions of minimum and maximum reflectivities as a function of wavelength and the number of bilayers again display behavior consistent with Eqs. (1) and (2). The first minimum of the five-bilayer film, the first maximum of the ten-bilayer film, and the second minimum of the 15-bilayer film occur at the same wave number, approximately 1.8 μm^{-1}. The minimum reflectivities at this wave number for the five-bilayer and 15-bilayer films are less than 0.2%.

For the largest size silica nanoparticles, the transmittances as a function of wave number of three silica

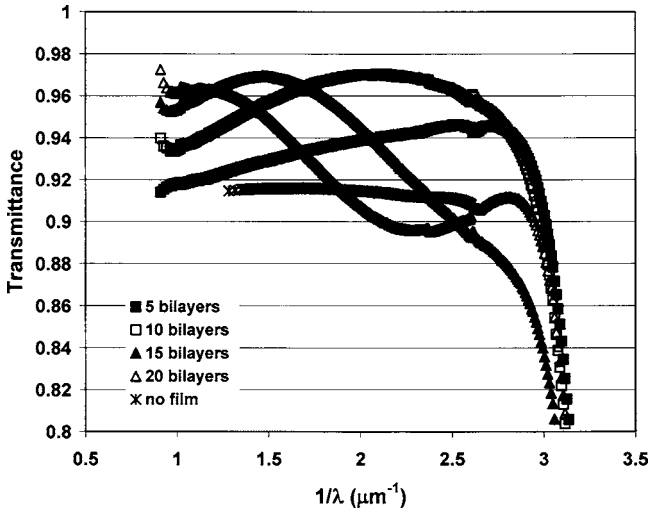

FIG. 1. Transmittance vs wave number (=$1/\lambda$) of films prepared with 15 nm average diameter silica nanoparticles (*p*H=7)/PAH(*p*H=7) for 5, 10, 15, and 20 bilayers. Also shown is the transmittance of a bare glass slide without any film.

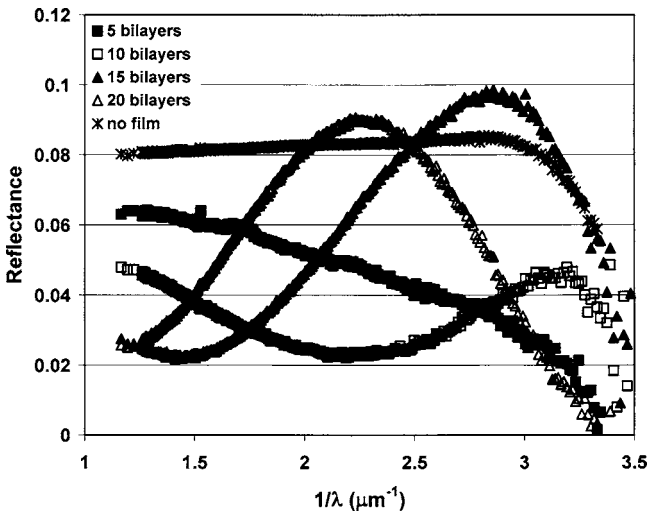

FIG. 2. Reflectance vs wave number of films prepared with 15 nm average diameter silica nanoparticles (*p*H=7)/PAH(*p*H=7) for 5, 10, 15, and 20 bilayers. Also shown is the reflectance of a bare glass slide without any film.

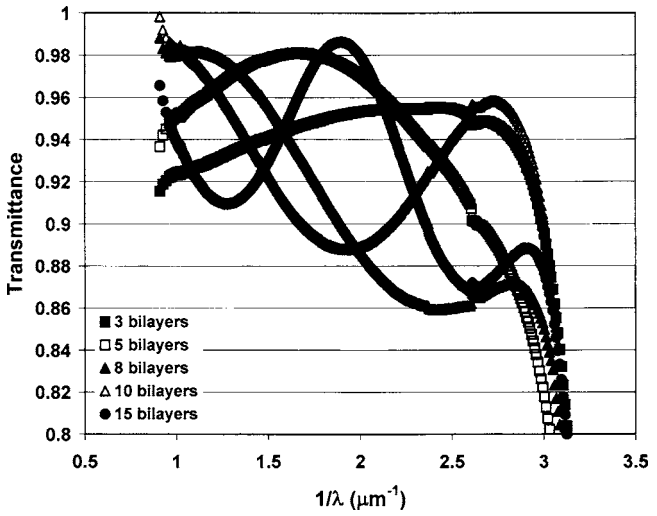

FIG. 3. Transmittance vs wave number of films prepared with 45 nm average diameter silica nanoparticles (pH=9)/PAH(pH=7) for 3, 5, 8, 10, and 15 bilayers.

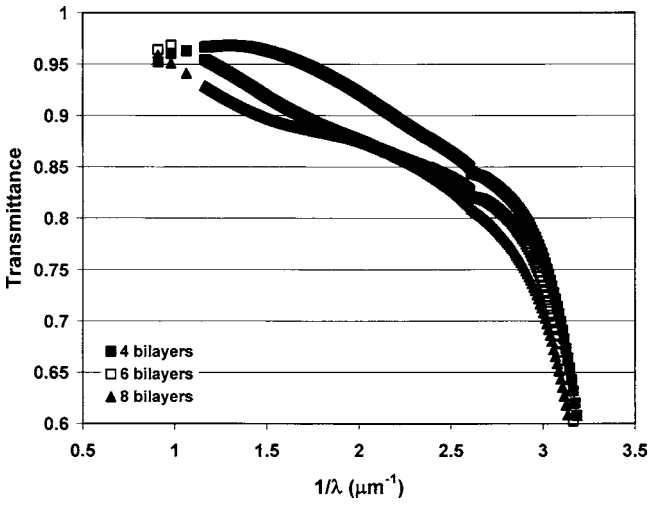

FIG. 5. Transmittance vs wave number of films prepared with 85 nm average diameter silica nanoparticles (pH=9)/PAH(pH=9) for 4, 6, and 8 bilayers.

(85 nm; pH=9)/PAH(pH=9) films having four, six, and eight bilayers are shown in Fig. 5 and the reflectances of the same samples are shown in Fig. 6. The effect of diffuse scattering on the interference fringes is visible in the transmission data for films prepared with 45 nm diameter silica nanoparticles, but is more evident in these films prepared with the 85 nm diameter nanoparticles. The interference fringes are superimposed on a monotonic decrease in the transmittance with increased wave number before the abrupt decrease associated with the silica absorption edge at 3.0 μm^{-1}. The effect of diffuse scattering also can be seen on the interference minima in the reflectances of the four- and eight-bilayer films. The first minima of the four-bilayer film, between wave numbers of 1.4 and 1.5 μm^{-1}, is less than 0.2%, while the second minima of the eight-bilayer film at 2.5 μm^{-1} is greater than 1.2%. The extinction of the incident light provides a measure of the diffuse scattering and will be discussed next.

B. Extinction measurements on films prepared with 15, 45, and 85 nm nanoparticles

In addition to the forward-transmitted and the specularly reflected light intensities, a fraction of the normal incident intensity on our films is absorbed and a fraction is scattered diffusely. The sum of the absorbed and diffusely scattered fractions, the extinction, is given by $1-R-T$, where R and T are the fractions of specularly reflected and forward-transmitted intensities, respectively. The absorbed fraction is negligible in our measurements for wave numbers less than the silica absorption edge at 3.0 μm^{-1} and, therefore, below this edge, the fraction $1-R-T$ is a measure of the diffusely scattered intensity. The extinctions versus $(1/\lambda)^4$ (λ =334–700 nm) for silica(15 nm; pH=7)/PAH(pH=7), silica(45 nm; pH=9)/PAH(pH=7), and silica(85 nm; pH =9)/PAH(pH=9) are shown in Figs. 7, 8, and 9, respectively. The data are plotted versus $(1/\lambda)^4$ to distinguish possible contributions from Rayleigh scattering at long wave-

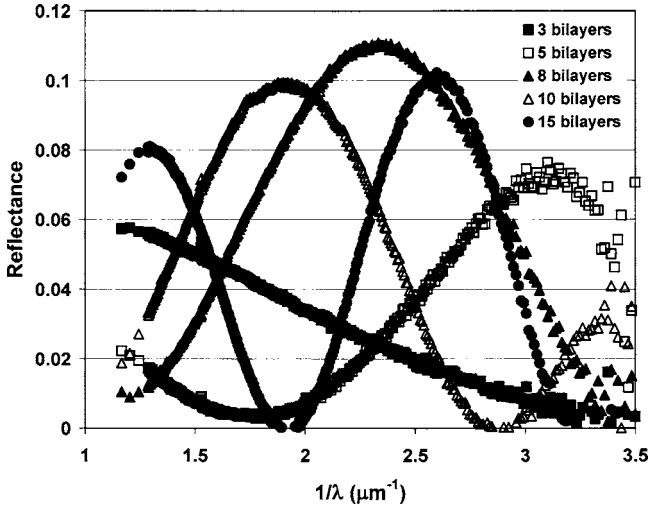

FIG. 4. Reflectance vs wave number of films prepared with 45 nm average diameter silica nanoparticles (pH=9)/PAH(pH=7) for 3, 5, 8, 10, and 15 bilayers.

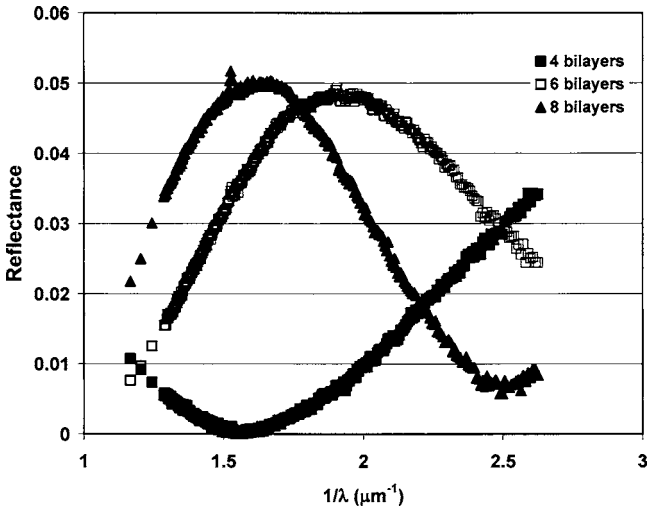

FIG. 6. Reflectance vs wave number of films prepared with 85 nm average diameter silica nanoparticles (pH=9)/PAH(pH=9) for 4, 6, and 8 bilayers.

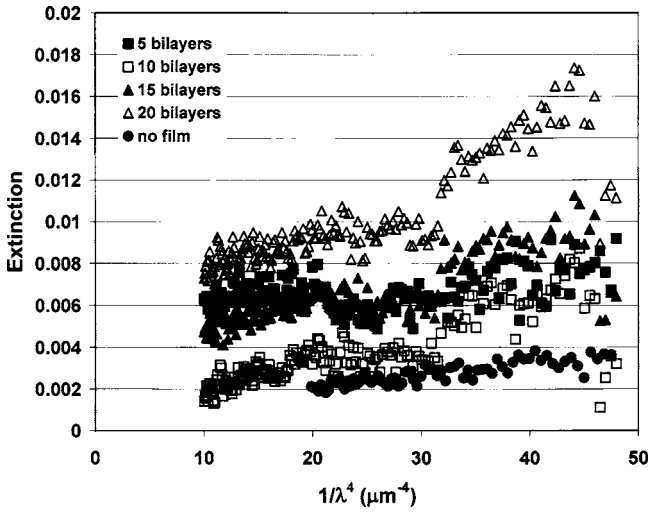

FIG. 7. Extinction vs $(1/\lambda)^4$ of films prepared with 15 nm average diameter silica nanoparticles (pH=7)/PAH(pH=7) for 5, 10, 15, and 20 bilayers. Also included in the figure is the extinction of a slide with no film.

length. The extinction versus $(1/\lambda)^4$ for a clean microscope slide also is plotted in Fig. 7 for comparison.

The extinction for each film and for the clean slide is quite linear in $1/\lambda^4$ over the wavelength region shown, suggestive of Rayleigh scattering at long wavelength. But the increasing extinction drops below a linear extrapolation of the initial dependence for $1/\lambda > 2.2\ \mu m^{-1}$ and then increases rapidly above the absorption edge. The linear dependence of the diffuse scattering on $1/\lambda^4$ will change as the wave number increases from the Rayleigh to the Mie scattering regime. But it is unclear why this change would produce the dip in extinction between 2.2 and 3.2 μm^{-1} that we observe.

C. Film thickness, void fraction, and index of refraction from ellipsometry

The thicknesses, void fractions, and indices of refraction of the films were measured with a J.A. Woolam variable angle spectral ellipsometer at two spots on each sample. The measurements were analyzed in terms of the Maxwell-Garnett (MG) effective-medium approximation.[15] We assumed, consonant with the Maxwell-Garnett approximation, that the films consisted of air voids in a homogeneous silica medium. The optical properties of silica were taken from Ref. 16. The remaining two parameters of the MG equation, the thickness of the film and the volume fraction of void, were iterated until the mean-square error between model and data was minimized. We also analyzed our results in terms of the symmetrical Bruggeman equation,[17] and obtained the same results within 1%.

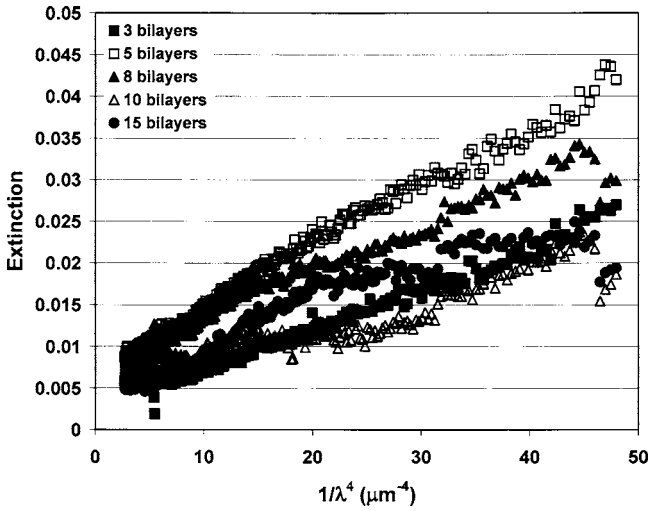

FIG. 8. Extinction vs $(1/\lambda)^4$ of films prepared with 45 nm average diameter silica nanoparticles (pH=9)/PAH(pH=7) for 3, 5, 8, 10, and 15 bilayers.

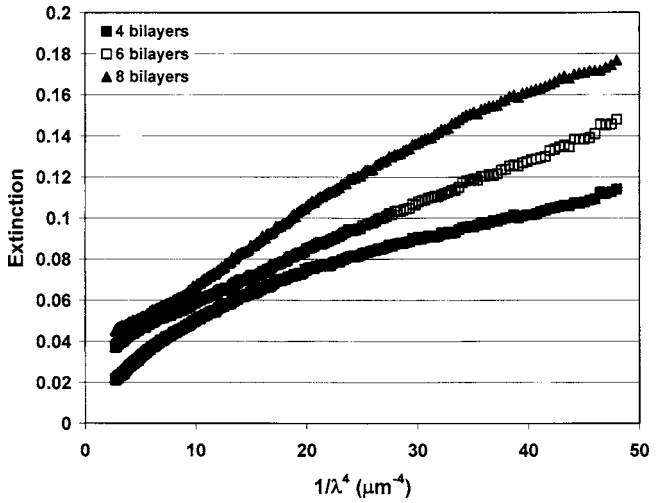

FIG. 9. Extinction vs $(1/\lambda)^4$ of films prepared with 85 nm average diameter silica nanoparticles (pH=9)/PAH(pH=9) for 4, 6, and 8 bilayers.

The derived thicknesses of the silica(15 nm; pH =7)/PAH(pH=7), silica(45 nm; pH=9)/PAH(pH=7), silica(45 nm; pH=9)/PAH(pH=9), and silica(85 nm; pH =9)/PAH(pH=9) films as a function of the number of bilayers are shown in Fig. 10. The solid lines through each data set are the linear regression fits with $R^2 \geqslant 0.96$ for all four

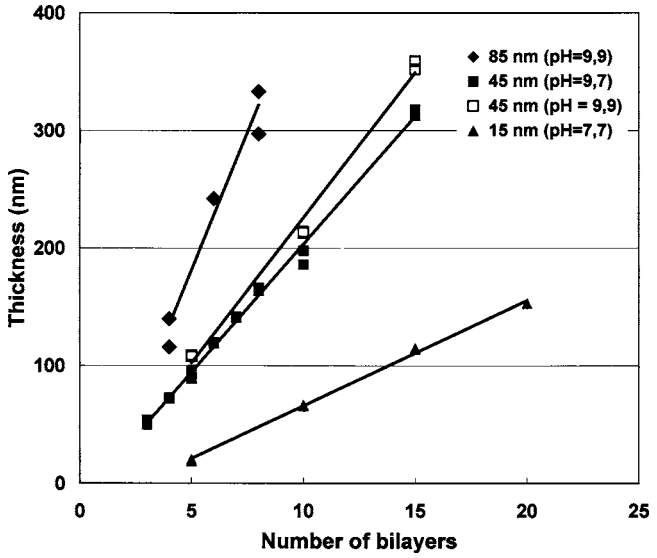

FIG. 10. Film thickness vs the number of bilayers for 15 nm average diameter silica nanoparticles (pH=7)/PAH(pH=7), 45 nm average diameter silica nanoparticles (pH=9)/PAH(pH=7), 45 nm average diameter silica nanoparticles (pH=9)/PAH(pH=9), and 85 nm average diameter silica nanoparticles (pH=9)/PAH(pH=9).

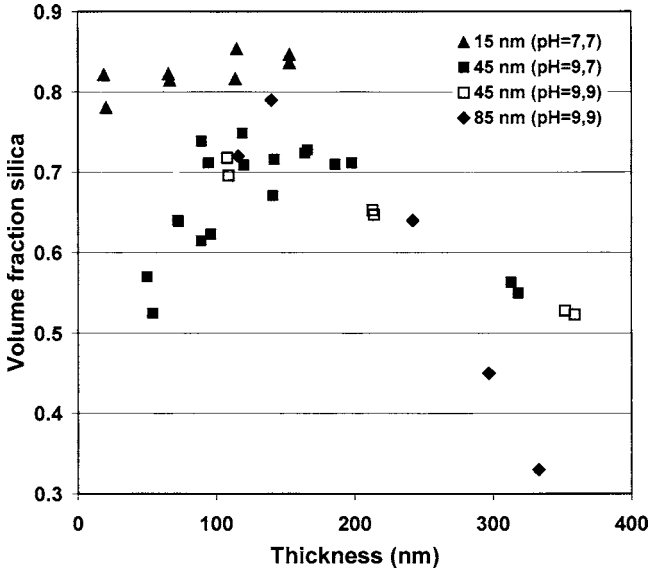

FIG. 11. Volume fraction of silica, from Maxwell-Garnett modeling of ellipsometry measurements, vs the number of bilayers for 15 nm average diameter silica nanoparticles (pH=7)/PAH(pH=7), 45 nm average diameter silica nanoparticles (pH=9)/PAH(pH=7), 45 nm average diameter silica nanoparticles (pH=9)/PAH(pH=9), and 85 nm average diameter silica nanoparticles (pH=9)/PAH(pH=9).

data sets. The derived slopes for silica(15 nm; pH =7)/PAH(pH=7), silica(45 nm; pH=9)/PAH(pH=7), silica(45 nm; pH=9)/PAH(pH=9), and silica(85 nm; pH =9)/PAH(pH=9) are 9.0, 22, 25, and 47 nm/bilayer, respectively. The derived intercepts for the same film sets are −24, −14, −21, and −52 nm, respectively.

The volume fractions of silica (equal to 1 minus the void fraction) in the silica(15 nm; pH=7)/PAH(pH=7), silica(45 nm; pH=9)/PAH(pH=7), silica(45 nm; pH =9)/PAH(pH=9), and silica(85 nm; pH=9)/PAH(pH=9) films as a function of the film thickness are shown in Fig. 11. The volume fractions of silica in the silica(15 nm; pH =7)/PAH(pH=7) films are independent of the number of bilayers within experimental scatter and equal to 0.82±0.02. The volume fractions of silica for silica(45 nm; pH =9)/PAH(pH=7) films increase monotonically up to a volume fraction of 0.7 at a thickness of approximately 100 nm and then, after remaining roughly constant between 100 and 200 nm thickness, decrease to a volume fraction of 0.55 for the last two data points with thickness of 320 nm. The data are less complete for silica(45 nm; pH=9)/PAH(pH=9) films, but displays the same qualitative trend seen in the data for silica(45 nm; pH=9)/PAH(pH=7). The volume fractions of silica in films prepared with 85 nm silica nanoparticles have a similar dependence on thickness as films silica(45 nm; pH=9)/PAH(pH=7) and silica(45 nm; pH =9)/PAH(pH=9).

In order to understand better the structure of our films, we prepared a series of one-, two-, three-, and ten-bilayer films of silica(45 nm; pH=9)/PAH(pH=7) that were coated with a 5-nm-thick film of gold, and then examined by field-emission scanning electron microscope (SEM) (LEO 1550). The SEM images are shown in Figs. 12(a)–12(d). Beginning with the one-bilayer film [Fig. 12(a)], several features are evident. First, the PAH polymer between the silica nanoparticle layers is not resolved, as would be expected since the typical thickness of PAH layers under this deposition condition is ~1 nm. Second, the silica nanoparticles are uniformly spherical in shape and the nanoparticle size distribution is quite broad. And, third, the nanoparticles aggregate in small clusters with significant space between the clusters. The SEM micrographs show that this void space between aggregates initially decreases with increasing number of bilayers.

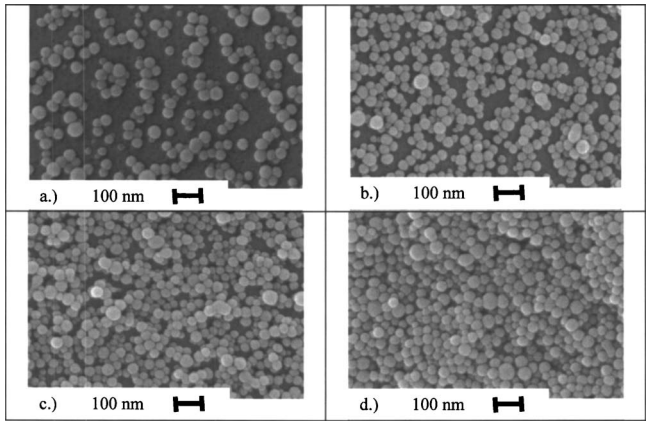

FIG. 12. SEM micrographs of films prepared from 45 nm average diameter silica nanoparticles (pH=9)/PAH(pH=7) for (a) one bilayer, (b) two bilayers, (c) three bilayers, and (d) ten bilayers.

The indices of refraction for the silica(15 nm; pH =7)/PAH(pH=7), silica(45 nm; pH=9)/PAH(pH=7), silica(45 nm; pH=9)/PAH(pH=9), and silica(85 nm; pH =9)/PAH(pH=9) films as a function of the film thickness are shown in Fig. 13. The indices of refraction and the silica volume fractions are correlated through the Maxwell-Garnet analysis of the ellipsometry measurements. The indices of refraction of all the films are less than the index of bulk silica as one would expect for a mixture of silica and void interstices.

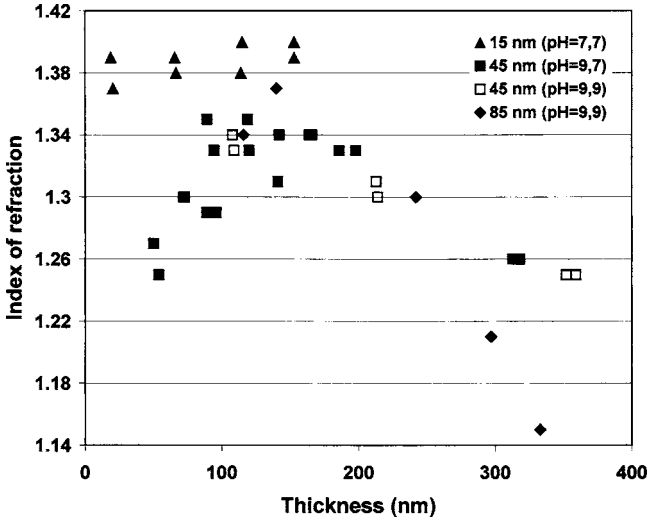

FIG. 13. Index of refraction vs the number of bilayers for 15 nm average diameter silica nanoparticles (pH=7)/PAH(pH=7), 45 nm average diameter silica nanoparticles (pH=9)/PAH(pH=7), 45 nm average diameter silica nanoparticles (pH=9)/PAH(pH=9), and 85 nm average diameter silica nanoparticles (pH=9)/PAH(pH=9).

The variation of the indices with respect to the film thickness for silica(15 nm; pH=7)/PAH(pH=7) films is not statistically significant. The average index of refraction for these films is 1.39±0.01. As a function of wavelength, the indices of refraction decrease by approximately 1% from the UV to the near IR as one would expect for silica. The decrease is not as large as occurs for pure silica because the film is diluted with void space which has a wavelength-independent index of refraction.

The indices of refraction for the silica(45 nm; ph =9)/PAH(pH=7) films as a function of film thickness increase monotonically up to a film thickness of approximately 100 nm, level off between thicknesses equal to 100 and 200 nm, and then decrease for films thicker than 200 nm, mirroring the behavior of the volume fraction of silica in these films. Though less data exists for the indices of refraction of silica(45 nm; pH=9)/PAH(pH=9) films, the dependence between index and film thickness is qualitatively similar to the dependence seen in the more extensive data set of silica(45 nm; pH=9)/PAH(pH=7). The indices for both silica(45 nm; pH=9)/PAH(pH=7) and silica(45 nm; pH =9)/PAH(pH=9) films decrease by $\leqslant$2% for wavelengths between λ=400 nm and λ=700 nm.

The indices of refraction for silica(85 nm; pH =9)/PAH(pH=7) have qualitatively the same dependence on film thickness, within experimental scatter, as the indices for films prepared with silica(45 nm; pH=9)/PAH(pH=7) and silica(45 nm; pH=9)/PAH(pH=9) nanoparticles. The indices for silica(85 nm; pH=9)/PAH(pH=7) films also decrease by 1%–2% for wavelengths between λ=400 nm and λ=700 nm.

IV. DISCUSSION

A. Film thickness

The incremental increases in film thickness per bilayer for silica(15 nm; pH=7)/PAH(pH=7), silica(45 nm; pH =9)/PAH(pH=7), silica(45 nm; pH=9)/PAH(pH=9), and silica(85 nm; pH=9)/PAH(pH=9) films are 9.0, 22, 25, and 47 nm, respectively. The respective ratios of incremental bilayer thicknesses to average nanoparticle diameters are 0.60, 0.49, 0.56, and 0.55, respectively. For a close-packed fcc crystal of hard spheres, the equivalent quantity is the ratio of the separation between the (111) planes to particle diameter, which is $\sqrt{2}/3$=0.816. Our measured ratios of bilayer thickness to nanoparticle diameter are significantly smaller because the nanoparticles do not form a close-packed monolayer at each deposition step. The average areal number densities of the bilayers in our films, relative to the maximum packing density of a hcp layer for equal diameter spheres, can be estimated from our data, as discussed below, and lies between 0.25 and 0.75.

Lvov *et al.* measured the incremental increase in thickness of films prepared from 25, 45, and 78 nm silica nanoparticles from the shift in frequency of a quartz-crystal microbalance as the film layers were deposited. They prepared their films from silica solutions with four different concentrations of silica nanoparticles (0.1, 1.0, 10, and 100 mg/ml). Based on scaling their data with respect to the concentration of silica nanoparticles in the colloidal solutions, we find from their data an incremental thickness to particle diameter of 0.61, 0.57, and 0.66 for 15, 45, and 85 nm average diameter silica nanoparticles, respectively. Their ratios are slightly higher than ours for all three diameter nanoparticles, but the difference is not statistically significantly.

We consider next the difference between films prepared with 45 nm diameter silica nanoparticles, but with different pH's for the PAH solutions. The thicknesses per bilayer of 45 nm silica films prepared with PAH solutions with pH=7 and pH=9 are 22 and 25 nm, respectively. Shiratori and Rubner found that the thickness of weak polyelectrolytes layers depends sensitively on pH.[18] In a study creating sequential multilayers of the weak polyelectrolytes poly(acrylic acid) (PAA) and PAH, they found that the marginal increase in thickness associated with a single PAH layer was less than 0.5 nm when the polycation solution pH=7 and approximately 5.0 nm when the solution pH=9. Given the experimental variability, this difference of 4.5 nm/bilayer is in rough agreement with the difference of 3 nm/bilayer that we found between bilayers prepared with PAH layers deposited at pH=9 versus bilayers prepared with PAH layers deposited at pH=7.

B. Void fraction and index of refraction

The index of refraction of our films can be modeled in the ellipsometry analysis by the Maxwell-Garnett effective-medium approximation, as discussed above. The volume fraction of silica in the film is an input parameter of this model and correlates closely with the index of refraction. The silica volume fractions as a function of film thickness are significantly larger for silica(15 nm; pH=7)/PAH(pH =7) films relative to silica(45 nm; pH=9)/PAH(pH=7), silica(45 nm; pH=9)/PAH(pH=9), and silica(85 nm; pH =9)/PAH(pH=9) films (see Fig. 11). The indices of refraction as a function of film thickness display the same qualitative difference between films prepared with 15 nm average diameter nanoparticles versus films prepared with 45 and 85 nm average diameter nanoparticles (see Fig. 13). The volume fractions and indices are constant, within experimental uncertainty, for films prepared with 15 nm diameter nanoparticles, while the volume fractions and indices of films prepared with 45 and 85 nm diameter nanoparticles appear to have the same functional dependence on thickness. The refractive indices and volume fractions reach a maximum value in silica(45 nm; pH=9)/PAH(pH=7) and silica (45 nm; pH=9)/PAH(pH=9) films that are 100–150 nm thick, then decrease in thicker samples. The volume fractions and refractive indices of silica(85 nm; pH=9)/PAH(pH =9) films are similar to those for the films prepared with 45 nm average diameter nanoparticles, within experimental scatter. We discuss next an exact relation between the volume fraction of a film and the average areal number density of the bilayers in the film.

The relation between the thicknesses of the bilayers and the volumes of each silica nanoparticle in the film is given by

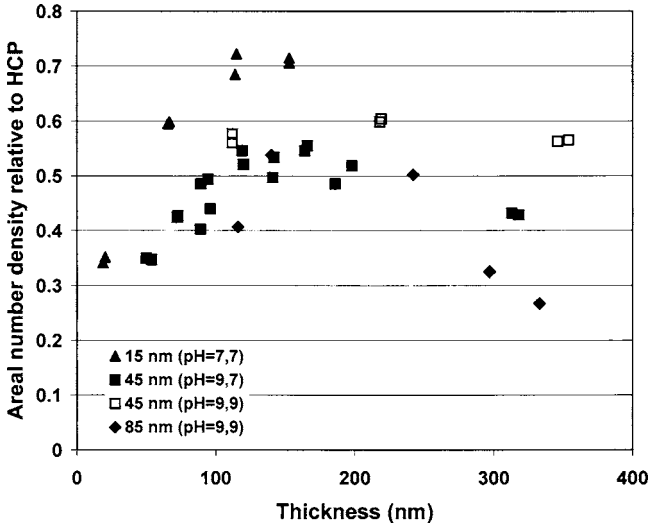

FIG. 14. The areal number density, relative to a hexagonal close packing of monodispersed spheres, vs film thickness for films prepared with 15 nm average diameter silica nanoparticles (pH=7)/PAH(pH=7), 45 nm average diameter silica nanoparticles (pH=9)/PAH(pH=7), 45 nm average diameter silica nanoparticles (pH=9)/PAH(pH=9), and 85 nm average diameter silica nanoparticles (pH=9)/PAH(pH=9).

$$f_{\text{silica}} A \sum_{i=1}^{n} t_i = \sum_{i=1}^{N} \nu_i, \tag{3}$$

where f_{silica} is the volume fraction of silica in the film, A is the area of the film, n is the number of bilayers, t_i is the thickness of the ith bilayer, N is the total number of silica nanoparticles in the film, and ν_i is the volume of the ith nanoparticle. From this relation it follows that

$$f_{\text{silica}} t_{\text{avg}} = \sigma_{\text{avg}} \nu_{\text{avg}}, \tag{4}$$

where $t_{\text{avg}}=(\Sigma t_i)/n$ is the average thickness of a bilayer, $\sigma_{\text{avg}}=N/nA$ is the average areal number density of a bilayer, and $\nu_{\text{avg}}=(\Sigma \nu_i)/N$ is the average volume of the nanoparticles.

We obtain the average thickness of a film from our linear regression analysis of the thickness versus number of bilayers in Fig. 10. We assume that the average volume of the nanoparticles in the films is $\pi D_{\text{avg}}^3/6$ where D_{avg} is the average diameter of the nanoparticles in the colloidal suspension from which the film was prepared. While the average diameter of nanoparticles in the film and in the colloidal suspension may be different because the adsorption of different size nanoparticles from the suspension on to the film may not be uniform, we assume here that the average nanoparticle diameter is the same on the film and in the colloidal suspension. We have measured the volume fraction of silica in the films by ellipsometry based on an analysis of the data in terms of the Maxwell-Garnett effective-medium approximation. Thus, the average areal number density of the bilayers can be calculated from Eq. (4). The results are plotted, versus the film thickness, in Fig. 14 for films prepared with 15, 45, and 85 nm average diameter silica nanoparticles. We have normalized the calculated areal number density to the maximum possible areal number density given by the areal number density of hcp monodispersed spheres, that is, $2/\sqrt{3}D^2$, where D is the diameter of the spheres.

The normalized areal number densities for all three sizes of nanospheres range roughly from 0.25 to 0.75. The normalized areal number densities of silica(15 nm; pH =7)/PAH(pH=7) and silica(45 nm; pH=9)/PAH(pH=7) films increase to a maximum of approximately 0.7 and 0.5, respectively. The normalized areal number densities of silica (45 nm; pH=9)/PAH(pH=7) films, then decrease to approximately 0.4 for the thickest films. The normalized areal number densities of silica(45 nm; pH=9)/PAH(pH=9) films do not change significantly with film thickness and are equal to 0.58 ± 0.02. The normalized areal number densities of silica(45 nm; pH=9)/PAH(pH=7) and silica (85 nm; pH=9)/PAH(pH=9) films are the same within experimental scatter for a given film thickness.

For fixed total adsorption time, the areal number density of silica nanoparticles on a film surface depends on the rate the nanoparticles impinge on the surface from the colloidal suspension while the film layer is deposited and on the probability that the impinging nanoparticles adsorb on the surface. The rate, nanoparticles are incident on the surface, depends on the concentration and diffusion rate of nanoparticles in the suspension. The diffusion rate of the nanoparticles in the suspension, in turn, depends on their size. The adsorption of the nanoparticles on the film surface depends on the interparticle potential energy between silica nanoparticles and the interparticle potential energy between silica nanoparticles and the polycation layer. The aggregation of the silica nanoparticles on the film surface depends, also, on the lateral diffusion of the nanoparticles that have adsorbed on the film surface. The rate nanoparticles are incident from the suspension on to the film surface does not depend on the number of bilayers that have been deposited and, hence, the change in the areal number density with number of bilayers (or film thickness) is governed by the adsorption probability on the surface and subsequent diffusion of nanoparticles adsorbed on the film.

The total interparticle potential energy between silica nanoparticles is a sum of terms.[19] The two critical terms that constitute the DLVO theory for the stability of colloidal particles suspended in polar fluids are the attractive long-range van der Waals interaction and the repulsive electrostatic interaction between like-charged particle surfaces. The same two terms plus the attractive electrostatic interaction between the surface charge on the silica nanoparticles and the polycation layer are the critical terms governing the lateral ordering of the nanoparticles in the bilayers. From the SEM micrograph for a one-bilayer film of silica(45 nm; pH =9)/PAH(pH=7), the influence on the areal number density of the attractive van der Waals and repulsive electrostatic interaction is evident [see Fig. 12(a)]. A few solitary nanoparticles exist on the substrate, but most nanoparticles are in aggregations of two to approximately ten nanoparticles due to the attractive interaction. Void spaces exist between the islands of nanoparticles due to repulsive interaction. What is not clear from the SEM micrographs is the nature of the void spaces in films with two or more bilayers [Figs.

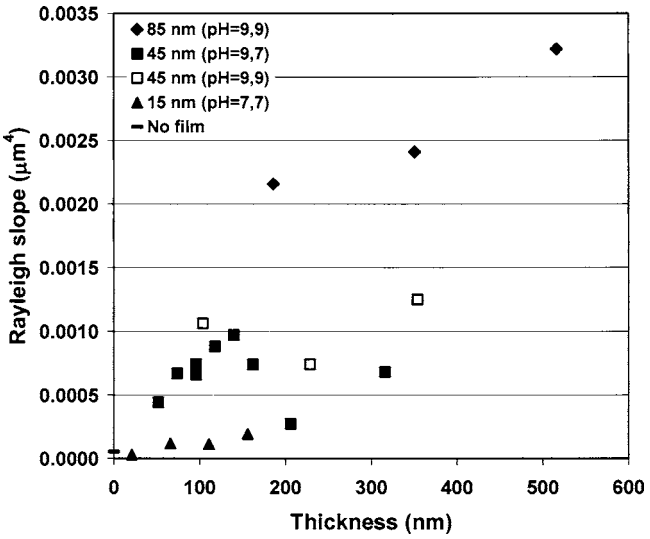

FIG. 15. The Rayleigh slope vs thickness for films prepared with 15 nm average diameter silica nanoparticles (pH=7)/PAH(pH=7), 45 nm average diameter silica nanoparticles (pH=9)/PAH(pH=7), 45 nm average diameter silica nanoparticles (pH=9)/PAH(pH=9), and 85 nm average diameter silica nanoparticles (pH=9)/PAH(pH=9). The Rayleigh slope for a substrate with no film is shown at zero thickness.

12(b)–12(d)]. After the silica nanoparticles in the first bilayer are covered with the polycation layer, the silica nanoparticles in the second bilayer fill in some of the void spaces that existed in the first bilayer [see Fig. 12(b)]. But one cannot distinguish clearly in the micrograph those nanoparticles that are in the first bilayer from those nanoparticles in the second bilayer. But the initial increase in the average areal number density with film thickness (Fig. 14) is consistent with the infill of nanoparticles into existing void space with each deposition step that is evident from Figs. 12(a) and 12(b). What is not clear and will require further research is the decrease in areal number density for films that are thicker than approximately 150 nm.

C. Diffuse scattering

We consider now the initial, linear slope for the extinction versus $(1/\lambda)^4$ (Figs. 7, 8, and 9 for films prepared with 15, 45, and 85 nm average diameter silica nanoparticles, respectively) and will call it the "Rayleigh slope." We fit this portion of the data by linear regression analysis and show a plot of the derived slopes versus the thickness of the films in Fig. 15. It is evident from this plot that the Rayleigh slope (RS) increases with increasing diameter of the silica nanoparticles in the film. Also, the dependence between the RS and film thickness appears to change when the films become thicker than approximately 150 nm. The Rayleigh slopes generally increase with increasing film thickness for films that are less than ~150 nm thick, while the Rayleigh slopes of films that are greater than ~150 nm thick show no clear dependence on thickness, but instead vary randomly with thickness. We suggest that the primary source of Rayleigh scattering is the roughness of the film surface rather than the variability of the refractive index in the bulk of the film. The distinctive dependence of the diffuse scattering on wavelength can arise if either the rms variation in the surface height or the scale of inhomogeneities in the bulk of the film is much smaller than the wavelength of light.[20,21] The surface roughness and the variation in the bulk index of refraction will scale with the size of the nanoparticles in the film and, therefore, the observed increase in scattering with increasing diameter nanoparticles is consistent with both scattering mechanisms. But the intensity of Rayleigh scattering will be independent of the thickness of the film in the case of roughness scattering and will be proportional to the thickness of the film if the source of scattering is in the bulk of the film. Thus, the observation that the Rayleigh slope does not depend on film thickness, within experimental scatter, for films greater than 150 nm thick and prepared with a given diameter silica nanoparticle strongly suggests a surface rather than a bulk source of the diffuse scattering. The increase in Rayleigh slope with increasing film thickness for films less than 150 nm thickness is probably because the surface roughness is increasing with film thickness and not because the Rayleigh scattering arises from a bulk source.

In conclusion, the observed dependence of Rayleigh scattering on the nanoparticle diameter is consistent with either surface roughness or inhomogeneities in the bulk dielectric constant of the films. But the random variation in the Rayleigh slope for films that are thicker than 150 nm is inconsistent with the bulk mechanism for Rayleigh scattering. We conclude, therefore, that the observed diffuse scattering is due to surface scatter and defer quantitative analysis of this scattering to further study.

V. SUMMARY

Low reflectivity coatings can be deposited efficiently by ionic self-assembly of silica nanoparticles, but two competing conditions on the size of the nanoparticles must be satisfied. The fraction of void volume in the film must be of order 0.3, in order to satisfy the criterion that the index of refraction of the film be equal to $n_c=\sqrt{n_1 n_2}$, where n_1 and n_2 are the refractive indexes of the media on each side of the film. This condition was not well satisfied by films created from 15 nm average diameter nanoparticles and the minimum reflectivity from these films was 2.2%. On the other hand, films prepared from 45 and 85 nm average diameter nanoparticles did have the necessary void volume fractions and the minimum reflectivities from these films were $\leqslant$0.2%. The peak transmittances of films prepared with 45 and 85 nm silica nanoparticles were greater than 98% and 96%, respectively. The peak transmittances of films prepared with the larger diameter silica nanoparticles were limited by diffuse scattering from the surface roughness of the films. The challenge in utilizing ionic self-assembly of silica nanoparticles for depositing antireflection films will be to reconcile the conflicting need for using larger nanoparticles to obtain the necessary void volume (for low index of refraction) and the concomitant diffuse scattering that arises from the rough surfaces created by these nanoparticles.

ACKNOWLEDGMENTS

We gratefully acknowledge significant discussions with Daniela Topasna and Paige Phillips at Luna Innovations. We

also thank Richard Zallen for his contributions and insights and Zhiyong Wang for expertise in ellipsometry.

[1]I. J. Iler, J. Colloid Interface Sci. **21**, 569 (1966).
[2]Y. M. Lvov and G. Decher, Crystallogr. Rep. **39**, 628 (1994).
[3]G. Decher, Science **277**, 1232 (1997).
[4]N. A. Kotov, in *Multilayer Thin Films*, edited by Gero Decher and Joseph B. Schlenoff (Wiley Interscience, New York, 2002), p. 207.
[5]P. T. Hammond, Curr. Opin. Colloid Interface Sci. **4**, 430 (2000).
[6]M. R. Bohmer, J. Colloid Interface Sci. **197**, 251 (1998).
[7]G. Bogdanovic, T. Sennerfors, B. Zhmud, and F. Tiberg, J. Colloid Interface Sci. **255**, 44 (2002).
[8]T. Sennerfors, G. Bogdanovic, and F. Tiberg, Langmuir **18**, 6410 (2002).
[9]Y. Lvov, K. Ariga, M. Onda, I. Ichinose, and T. Kunitake, Langmuir **13**, 6195 (1997).
[10]H. Hattori, Adv. Mater. (Weinheim, Ger.) **13**, 51 (2001).
[11]Y. Lvov, J. Rusling, D. L. Thomsen, F. Papadimitrakopoulos, T. Kawakami, and T. Kunitake, Chem. Commun. (Cambridge) **1998**, 1229.
[12]T. Yonezawa, S. Onoue, and T. Kunitake, Chem. Lett. **7**, 689 (1998).
[13]Z. Adamczyk, B. Siwek, M. Zembala, and P. Belouscher, Adv. Colloid Interface Sci. **48**, 151 (1994); Z. Adamczyk and P. Warszynski, *ibid.* **63**, 41 (1996); M. Bohmer, E. van der Zeeuw, and G. Koper, J. Colloid Interface Sci. **197**, 242 (1998); M. Miyahara, S. Watanabe, Y. Gotoh, and K. Higashitani, J. Chem. Phys. **120**, 1524 (2004); M. Bohmer, J. Colloid Interface Sci. **197**, 251 (1998); V. Privman, H. Frisch, N. Ryde, and E. Matijevic, J. Chem. Soc., Faraday Trans. **87**, 1371 (1991).
[14]W. Kern and D. A. Poutinen, RCA Rev. **31**, 187 (1970).
[15]J. C. Maxwell-Garnett, Philos. Trans. R. Soc. London **203**, 385 (1904); **205**, 237 (1906); also, see discussion of the effective medium approximation by R. Landauer, in *Electrical Transport and Optical Properties of Inhomogeneous Media*, edited by J. C. Garland and D. B. Tanner, AIP Conf. Proc. No. 40 (AIP, New York, 1978), p. 2.
[16]Edward D. Palik, *Handbook of Optical Constants of Solids I* (Academic, Orlando, 1985), p. 759.
[17]D. A. G. Bruggeman, Ann. Phys. **24**, 636 (1935).
[18]D. Yoo, S. S. Shiratori, and M. Rubner, Macromolecules **31**, 4309 (1998); S. S. Shiratori and M. F. Rubner *ibid.* **33**, 4213 (2000).
[19]R. French, J. Am. Ceram. Soc. **83**, 2117 (2000).
[20]J. M. Elson, H. E. Bennett, and J. M. Bennett, in *Applied Optics and Optical Engineering*, edited by R. R. Shannon and J. C. Wyant (Academic, New York, 1979), Vol. VII, p. 191.
[21]A. T. Young, Phys. Today **35**(1), 42 (1982).